ZEUS-pub-06-007-draft

Submitted to the
XXXIII International Conference on High Energy Physics
July 26 - August 2, 2006, Moscow, Russia

Abstract: - **Session: Beyond the Standard Model**

Search for stop production in R-parity-violating supersymmetry at HERA

ZEUS Collaboration

25th July 2006

Abstract

A search for stop production in R-parity-violating supersymmetry has been performed in e^+p interactions with the ZEUS detector at HERA using an integrated luminosity of 65 pb^{-1}. At HERA, the R-parity-violating coupling λ' allows resonant squark production $e^+d \to \tilde{q}$. Since the lowest mass squark state in most supersymmetry models is the light stop, $\tilde{t}$, this search concentrated on production of $\tilde{t}$, followed either by a direct R-parity violating decay, or by the gauge decay to $b\tilde{\chi}^+$. No evidence for stop production was found and limits were set on λ'_{131} as a function of the stop mass in the framework of the Minimal Supersymmetric Standard Model. The results have also been interpreted in terms of constraints on the parameters of the minimal Supergravity model.

1 Introduction

Many extensions of the Standard Model (SM) require a new fundamental symmetry between bosons and fermions, known as *supersymmetry* (SUSY) [1]. This symmetry, hypothesizing the existence of supersymmetric partners of the SM particles, with similar properties but with spin changed by one half, controls the divergent higher-order loop corrections of the Higgs boson mass. Despite numerous searches for such new particles, no evidence has been observed, indicating that supersymmetry, if exists, becomes manifest at scales beyond the present experimental limit. Since SUSY involves so many parameters, different experimental techniques typically complement each other.

One important quantum number in supersymmetric models is R-parity (R_p). Its conservation ensures the conservation of both lepton and baryon number. Most of the searches performed at colliders drew conclusions under the assumption of R_p conservation. Nevertheless, the most general supersymmetric extension of the SM Lagrangian contains terms which violate R_p and some of the possible R_p-violating ($\not{R}_p$) scenarios are compatible with the present experimental constraints.

One of the most remarkable consequences of $\not{R}_p$ scenarios is the possibility to resonantly produce single SUSY particles at colliders. Electron-proton collisions at HERA are well suited to the search for squarks, the scalar supersymmetric partners of quarks, since such states can be produced by an appropriate coupling of the incoming lepton and a quark in the proton.

In most of the SUSY scenarios, the squarks of the third generation are the lightest; the present analysis is aimed to search for the stop, $\tilde{t}$, the supersymmetric partner of the top quark. At HERA, the stop can be produced resonantly via the interaction $e^+d \to \tilde{t}$, up to the ep centre-of-mass energy $\sqrt{s} = 320\,\text{GeV}$. The stop decay can lead to distinctive topologies with a high-energy electron[1] or neutrino and hadronic jets, which can be efficiently separated from the SM background.

2 Stop phenomenology

The R-parity, defined as $R_p = (-1)^{3B+L+2S}$, is a multiplicative quantum number which is 1 for particles and -1 for sparticles (B, L and S denote baryon number, lepton number and spin, respectively). R-parity conservation would imply that supersymmetric particles are always pair produced and the lightest supersymmetric particle (LSP) is stable, a good candidate for cold dark matter.

[1] Here electron is used generically to indicate both positron and electron.

If R-parity is violated, it is possible to create single sparticles which decay back to SM particles [2]. The $\not{R}_p$ terms in the SUSY superpotential are given by:

$$W_{\not{R}_p} = \lambda_{ijk} L_i L_j \overline{E}_k + \lambda'_{ijk} L_i Q_j \overline{D}_k + \lambda''_{ijk} U_i \overline{D}_j \overline{D}_k \tag{1}$$

where the subscripts i,j,k are the generation indices, L_i denotes the $SU(2)$ doublet lepton superfield, E_i the $SU(2)$ singlet lepton superfield, Q_i the $SU(2)$ doublet quark superfield and D_i and U_i the $SU(2)$ singlet down- and up-type quark superfields. The dimensionless Yukawa couplings λ_{ijk}, λ'_{ijk}, λ''_{ijk} are free parameters of the model.

In the case of stop production in ep collisions, the only terms involved are those parameterized by the Yukawa coupling λ'_{131}. The partners of the left- and right-handed top, $\tilde{t}_L$ and $\tilde{t}_R$, can mix together in two mass eigenstates, $\tilde{t}_1$ and $\tilde{t}_2$, which, because of the large stop mass, are usually strongly non-degenerate. Due to the chiral properties of the SUSY superpotential (Eq. 1) only the $\tilde{t}_L$ state contributes to the stop production cross section. In the regime of narrow-width approximation (NWA), the production cross section for the lighter state $\tilde{t}_1$ is hence:

$$\sigma(e^+ p \rightarrow \tilde{t}_1) = \frac{\pi}{4s} \left(\cos\theta_{\tilde{t}} \cdot \lambda'_{131}\right)^2 d(M^2_{\tilde{t}_1}/s, M^2_{\tilde{t}_1}), \tag{2}$$

where $d(x, Q^2)$ is the parton density of the d quark in the proton and $\theta_{\tilde{t}}$ is the mixing angle between $\tilde{t}_1$ and $\tilde{t}_2$. In this paper only the lighter stop, $\tilde{t}_1$, denoted hereafter as $\tilde{t}$, has been considered since contributions from $\tilde{t}_2$ are negligible for all the considered scenarios.

The $\tilde{t}$ decays considered in this study, are the R_p-violating channel $\tilde{t} \rightarrow e^+ d$ and the R_p-conserving decays $\tilde{t} \rightarrow \tilde{\chi}^+_1 b$, where $\tilde{\chi}^+_1$ is the lightest chargino. These two channels provide a sufficiently large total branching ratio over all of the considered SUSY parameter space. The channel $\tilde{t} \rightarrow \tilde{\chi}^0_1 t$, where $\tilde{\chi}^0_1$ is the lightest neutrlino, contributes only at the highest stop masses, and even then it is below 10%. Branching ratios involving a heavier chargino or neutralino are small in most of the considered parameter space.

The considered decays, including the cascade from the $\tilde{\chi}^+_1$, are illustrated in Fig. 1. In the present paper only the hadronic W decays are considered, hence final states involving one positron with one (e-J) or more than one jets (e-MJ), and one neutrino and multiple-jets (ν-MJ) are studied.

The results have been interpreted in the contest of two different SUSY scenraios: the Minimal Supersymmetric Standard Model (MSSM) and the minimal Supergravity model (mSUGRA).

In the unconstrained $\not{R}_p$ Minimal Supersymmetric Standard Model (MSSM) [5] the branching ratios for stop decay as well as the masses of the neutralinos (mass eigenstates of the supersymmetric partners of neutral SM bosons), charginos and gluinos (supersymmetric partners of gluons) are determined by the following MSSM parameters: the mass term μ, which mixes the Higgs superfields; the soft SUSY-breaking parameters M_1, M_2 and M_3 for the $U(1)$, $SU(2)$ and $SU(3)$ gauginos, respectively; $\tan\beta$, the ratio of the vacuum expectation values of the two neutral scalar Higgs fields and the $\not{R}_p$ Yukawa couplings. The search for the stop was performed in the mass range $100 - 280\,\text{GeV}$. In order to minimize the number of free parameters, the assumptions listed below were made:

- no mixing between $\tilde{t}_L$ and $\tilde{t}_R$ ($\theta_{\tilde{t}} = 0$);
- only the Yukawa coupling λ'_{131} was assumed to be non-zero;
- SUSY scenarios in which the lightest neutralino $\tilde{\chi}^0_1$ is not the LSP or is lighter than 30 GeV were not considered since they have already been excluded by LEP results [6];
- the GUT relations [7] for the gaugino mass terms M_1, M_2 and M_3:

$$M_1 = \frac{5}{3}\tan^2\theta_W \cdot M_2, \tag{3}$$

$$M_3 = \frac{\alpha_S}{\alpha_{\text{EM}}}\sin^2\theta_W \cdot M_2 \tag{4}$$

  are assumed. As a consequence, the gluino is always heavier than $\tilde{t}$, so that the decay $\tilde{t} \to t\ \tilde{g}$ is kinematically forbidden;
- all the other sfermions (apart from the lighter stop) were assumed to have large masses that were fixed at 1 TeV.

The total branching ratio due to the considered decay channels is $\gtrsim 70\%$ for the range of parameters $|\mu| < 300\,\text{GeV}$ and M_2 between 100 and 300 GeV which was considered in this analysis.

Figure 2 shows the branching ratios for four representative points in the μ-M_2 plane involving very different masses for $\tilde{\chi}^0_1$ and $\tilde{\chi}^+_1$ and for λ'_{131} values equal to the limit given in Section 6.2. The dark band indicates the sum of the three considered channels for $2 < \tan\beta < 50$. The total branching ratio and the contribution of the three channels is shown for the value $\tan\beta = 6$. When the $\tilde{\chi}^+_1$ mass is larger than the stop mass, the $\not{R}_p$-violating decay (e-J) is the dominant channel, in the other cases the ν-MJ channel is typically the most relevant.

In the minimal supergravity model (mSUGRA) [8], the number of free parameters is further reduced by assuming two universal mass parameters at the GUT scale, m_0 and $m_{1/2}$, for all the sfermions and for all the gauginos, respectively. Radiative corrections are assumed to drive the Electro Weak Symmetry Breaking (REWSB) in this model, leading to consistency relations that allow to fix the complete model based only on m_0, $m_{1/2}$, the sign of μ, $\tan\beta$, and the common trilinear coupling A_0. In the range of parameters used in this analysis, $m_{1/2} < 180\,\text{GeV}$ and $m_0 < 300\,\text{GeV}$, the total branching ratio of the considered channel is in the range $0.4 - 0.8$ for $m_0 < 200\,\text{GeV}$. For larger values of m_0 it decreases rapidly since decay channels involving the heavier chargino, which are not considered in this study, become important.

3 Data sample and experimental set-up

The data used in this analysis were collected in the years 1999-2000. The total integrated luminosity was $65.1 \pm 1.1\ \text{pb}^{-1}$ of e^+p collisions. The proton and electron energies were $E_p^{beam} = 920\,\text{GeV}$ and $E_e^{beam} = 27.5\,\text{GeV}$, respectively, leading to a center-of-mass energy of $318\,\text{GeV}$.

A detailed description of the ZEUS detector can be found elsewhere [9]. A brief outline of the components that are most relevant for this analysis is given below.

Charged particles are tracked in the central tracking detector (CTD) [10], which operates in a magnetic field of $1.43\,\text{T}$ provided by a thin superconducting coil. The CTD consists of 72 cylindrical drift chamber layers, organized in 9 superlayers covering the polar-angle[2] region $15^\circ < \theta < 164^\circ$. The transverse-momentum resolution for full-length tracks is $\sigma(p_T)/p_T = 0.0058 p_T \oplus 0.0065 \oplus 0.0014/p_T$, with p_T in GeV.

The high-resolution uranium–scintillator calorimeter (CAL) [11] consists of three parts: the forward (FCAL), the barrel (BCAL) and the rear (RCAL) calorimeters. Each part is subdivided transversely into towers and longitudinally into one electromagnetic section (EMC) and either one (in RCAL) or two (in BCAL and FCAL) hadronic sections (HAC). The smallest subdivision of the calorimeter is called a cell. The CAL energy resolutions, as measured under test-beam conditions, are $\sigma(E)/E = 0.18/\sqrt{E}$ for electrons and $\sigma(E)/E = 0.35/\sqrt{E}$ for hadrons, with E in GeV.

The luminosity was measured using the bremsstrahlung process $ep \to ep\gamma$. The resulting small-angle energetic photons were measured by the luminosity monitor [12], a lead-scintillator calorimeter placed in the HERA tunnel at $Z = -107$ m.

[2] The ZEUS coordinate system is a right-handed Cartesian system, with the Z axis pointing in the proton beam direction, referred to as the "forward direction", and the X axis pointing left towards the centre of HERA. The coordinate origin is at the nominal interaction point. The pseudorapidity is defined as $\eta = -\ln\left(\tan\frac{\theta}{2}\right)$, where the polar angle, θ, is measured with respect to the proton beam direction.

4 Monte Carlo simulation

The signal processes were simulated with the Monte Carlo (MC) event generator SUSYGEN 3 [23]. It uses the exact matrix element for the production and for the decays of sparticles, includes initial and final state radiative corrections and is interfaced to PYTHIA 6.2 [13] for the hadronisation of the final state. The program SUSPECT 2.1 [35] is used to solve the REWSB consistency relations that determine the sparticle mass spectrum at the electro-weak scale assuming REWSB.

The dominant background process to the e-J and e-MJ channels is neutral current deep inelastic scattering (NC DIS). For the e-J channel, the background is due to $2 \rightarrow 2$ scatters between high-x quarks and the positron. Backgrounds to the e-MJ channel occurs in NC DIS events where multi-jet final states result from higher-order QCD effects.

The primary background to the ν-MJ channel comes from charged current deep inelastic scattering (CC DIS) with multiple jets from QCD radiation. An additional background source involves photoproduction events for which the measured transverse momentum is large due to energy mismeasurement.

The NC and CC events were simulated using the HERACLES 4.6.1 [14] program with the DJANGOH 1.1 [15] interface to the hadronization program and using the CTEQ5D [16] set of parton distribution functions (PDFs). In HERACLES, corrections for initial-state and final-state electroweak radiation, vertex and propagator corrections, and two-boson exchange are included. The colour-dipole model of ARIADNE 4.10 [17] was used to simulate the order α_S plus leading-logarithmic corrections to the quark-parton model. The MEPS model of LEPTO 6.5 [18], was used as a systematic check. Both programs use the Lund string model of JETSET 7.4 [19] for the hadronization.

Photoproduction events were simulated using the HERWIG 6.100 [20] generator, using the CTEQ4L [21] proton PDFs. Both direct and resolved photoproduction have been considered. In the direct case, all of the photon energy participates in the hard scattering, whereas, for the resolved process, only a fraction of the photon energy, associated with a parton constituent of the photon, participates in the hard subprocess. For the simulation of the resolved subprocess, the GRV-G [22] photon PDF was used.

5 Event selection

The signal events are characterised by a high-energy lepton in the final state. In the case of a positron in the final state (e-J and e-MJ channels), the trigger selection was based on a standard neutral current trigger which required a scattered electron, as used in searches for resonance states decaying to eq [25] and in ZEUS NC DIS studies [26]. For the neutrino case (ν-MJ channel), a trigger selection based on a missing P_T requirement and already employed in the ZEUS CC DIS analysis [27] was used.

The offline signal-search procedure was performed in two steps. Initially, a preselection was applied to select NC or CC events. Finally, more restrictive selections, optimized to get the best limits in the case of no signal, were applied.

5.1 Preselection for e^+ final states

The following conditions were designed to select a sample of high-Q^2 NC events, some of which were also used at the trigger level with a lower threshold:

- Z-coordinate of the event vertex compatible with an ep interaction, $|Z_{\rm vtx}| < 50$ cm;
- a high-energy positron reconstructed from calorimeter and tracking information [28]. A positron energy $E_e > 8\,{\rm GeV}$ was required. This cut was increased to $P_{T,e} > 20\,{\rm GeV}$ ($P_{T,e}$ is the transverse energy of the positron measured by the calorimeter) for very forward positrons ($\theta_e < 0.3$, where θ_e is the positron polar angle) which are outside the acceptance of the CTD;
- $45 < E - P_Z < 70\,{\rm GeV}$, where E and P_Z are are the total energy and the Z-component of the total momentum of the final-state. For NC DIS events, where only particles in the very forward direction escape detection, $E - P_Z \sim 2E_e^{\rm beam} = 55\,{\rm GeV}$;
- $Q^2_{\rm DA} > 1000\,{\rm GeV}^2$ and $0.2 < y_{\rm DA} < 0.98$, where $Q^2_{\rm DA}$ and $y_{\rm DA}$ are the DIS kinematic variables reconstructed using the double angle method [29]. The above conditions were imposed in order to restrict the search to a region where the signal is enhanced with respect to NC DIS and the reconstruction of the kinematic variables is reliable;
- $M_{eX} > 100\,{\rm GeV}$, where M_{eX} is the invariant mass of the positron and the hadronic system evaluated using the following relation that exploits the conservation of momentum and $(E - P_Z)$:
$$M^2_{eX} = 2E_e^{\rm beam} \sum_i (E + P_Z)_i. \tag{5}$$
The sum runs over the final-state positron and all other energy deposits with a polar angle > 0.1, to avoid the contributions from the proton remnant.

The bias and resolution of the reconstructed mass were evaluated using the signal MC. On average, the mass was slightly overestimated at low masses (3% at 100 GeV), while the agreement improved towards high masses ($<$ 1% above 150 GeV). The resolution was between 5% and 1.5% in the mass range $100 - 280$ GeV. After the preselection cuts, 2368 events remained, in good agreement with the expectation of the SM MC of 2430^{+90}_{-252} events, where the systematic uncertainties described in Section 6.1 dominates. The SM prediction is dominated by the NC DIS contribution.

Figure 3 shows the distributions of the transverse momentum of the scattered positron, $P_{T,e}$, $y_{\rm DA}$, $\log_{10}(Q^2_{\rm DA})$ and $P_{T,\rm antipar}/P_{T,\rm par}$ for data and MC; reasonable agreement is seen for all variables. The quantities $P_{T,\rm antipar}$ and $P_{T,\rm par}$ are the components of the hadronic system parallel and antiparallel to the axis defined by the direction of the hadronic P_T. The ratio $P_{T,\rm antipar}/P_{T,\rm par}$ is used in the final selection to separate one-jet events ($P_{T,\rm antipar}/P_{T,\rm par} \sim 0$) from multi-jet events ($P_{T,\rm antipar}/P_{T,\rm par} > 0$).

5.2 Preselection for ν final state

Events with a neutrino in the final state have a topology similar to CC DIS. The following selection cuts were applied in order to select a sample of high-Q^2 CC events and suppress the non-ep contribution:

- Z-coordinate of the event vertex compatible with an ep interaction, $|Z_{\rm vtx}| < 50$ cm;
- no reconstructed positron satisfying the same criteria used in e^+ final-state preselection;
- high missing transverse momentum, $P_{T,miss} > 20$ GeV;
- $0.2 < y_{\rm JB} < 0.95$, where $y_{\rm JB}$ is reconstructed using the Jacquet-Blondel method [30].

The analogue of Eq. 5 for the invariant mass of the ν-hadronic system was derived assuming that the missing P_T and $E - P_Z$ is due to a single neutrino:

$$M^2_{\nu X} = 2E_e^{\rm beam}\left(\sum_i (E+P_z)_i + P_t^2/(2E_e^{\rm beam}\,(1-y_{\rm JB}))\right). \qquad (6)$$

The sum runs over all the calorimeter energy deposits with a polar angle > 0.1, to exclude contribution from the proton remnant.

The mass resolution is between 10% and 3% in the mass range $100-280$ GeV. On average, the mass is slightly underestimated at high masses (1.5% at 280 GeV), while the agreement improves towards low masses ($< 1\%$ above 120 GeV). After the CC preselection cuts 265 events survived, in good agreement with the expectation of the SM MC of 277^{+18}_{-21}. The SM prediction is dominated by CC DIS events, with a small contribution coming from photoproduction processes.

Figure 4 shows the distributions of $P_{T,miss}$, $y_{\rm JB}$, $\log_{10}(Q^2_{\rm JB})$, where the Q^2_{JB} is reconstructed using the Jacquet-Blondel method, and $P_{T,antipar}/P_{T,par}$ for data and MC; reasonable agreement is observed for all the variables.

5.3 Final selection for e^+ final state

The final selection for the channels with a final-state positron was designed to further reduce the contamination from NC DIS by requiring high-Q^2 and high-y events. The following cuts were applied:

- $Q^2_{\rm DA} > 3000\,{\rm GeV}^2$,
- the y cut was adjusted as a function of the reconstructed mass, $y_{\rm DA} > 0.7 - 0.4$, in the mass range $100 - 280\,{\rm GeV}$. This cut exploits the different y-dependence of the NC DIS production, steeply decreasing as y^{-2}, and of a scalar resonance, which is flat in y.

Finally, a cut on $P_{T,{\rm antipar}}/P_{T,{\rm par}}$ was used to produce two samples enriched with either one-jet or multi-jet events. The e-J (e-MJ) final sample was defined requiring:

- $P_{t,{\rm antipar}}/P_{t,{\rm par}} < (>)\ 0.05$

Signal efficiencies were evaluated by generating samples of signal events using SUSYGEN for different values of the MSSM or mSUGRA parameters. For the e-J channel, the efficiencies ranged between $10 - 45\%$ in the mass range $100 - 260\,{\rm GeV}$ decreasing to 20% at $280\,{\rm GeV}$. For the MSSM scenario, the efficiencies for the e-MJ channel were in the range $5 - 25\%$ for stop masses between 200 and $280\,{\rm GeV}$ depending mainly on the masses of stop and chargino; the efficiency decreased towards lower and higher stop masses. For the mSUGRA scenario, the efficiencies for the e-MJ channel were in the range $5 - 15\%$ in most of the parameter space. The first two rows of Table 1 summarize the final cut values, numbers of events from data and SM MC and signal efficiency for the MSSM for e-J and e-MJ channels, respectively. Good agreement between the number of selected events and SM expectation is observed.

Figure 5a,b show the comparison between data and MC for mass distributions after the preselection and final selection for the e-J and e-MJ samples, respectively. The data distributions are well described by the SM simulation.

5.4 Final selection for ν final state

In order to enhance stop sensitivity and further reduce the contribution of CC DIS, the final selection requires:

- $y_{\rm JB} > 0.6$
- $P_{t,{\rm antipar}}/P_{t,{\rm par}} > 0.1$

For the MSSM scenario, the efficiencies were in the range 15−35% for stop masses between 180 and 280 GeV, depending mainly on the masses of stop and $\tilde{\chi}_1^0$; the efficiency decreased towards lower and higher stop masses. For the mSUGRA scenario, the efficiencies were in the range $5-20\%$ in most of the considered parameter space. Final cut values, numbers of events from data and SM MC and MSSM signal efficiency are summarized in third row of Table 1. The agreement between the number of selected events and the SM expectation is also good.

Figure 5c shows the comparison between data and MC for the mass distribution after the preselection and final selection for the ν-MJ channel. The MC simulation also in this case describes the data reasonably well.

6 Results

Since no evidence for stop production was found, limits at 95% CL were set using a Bayesian approach. The limits were set for two different SUSY scenarios: the unconstrained MSSM model and the mSUGRA model (see Section 2).

6.1 Systematic uncertainties

In the calculation of the upper limit on λ'_{131}, several sources of systematic uncertainties have been considered. The following systematic uncertainties on the SM background expectation were evaluated by considering the following sources:

- the uncertainty from the proton PDFs, evaluated using the procedure suggested by the CTEQ group [32] was ±4% for ν-MJ and ±2% for e-MJ and e-J;
- the uncertainty on the calorimeter energy scale of ±1% (±2%) for the electromagnetic (hadronic) section led to an uncertainty on the SM event rate of ±5% for ν-MJ and $^{+1\%}_{-3\%}$ for e-MJ and e-J;
- the use of MEPS instead of ARIADNE to simulate the QCD cascade led to an uncertainty of −3% for (ν-MJ) and −6% for (e-MJ) and (e-J) channels;
- the uncertainty in the integrated luminosity measurement was ±2.25%.

In addition, the following uncertainties related to the signal simulation were considered:

- the uncertainties in the signal efficiency due to interpolation between different SUSY scenarios was ±15%;

- the theoretical uncertainty on the signal cross section due to the uncertainty in the d quark parton density [32] in the proton varied from $\pm 3\%$ to $\pm 80\%$ for masses between 100 and 280 GeV.

6.2 Limits for MSSM model

Assuming the MSSM model, the upper limits on λ'_{131} were evaluated as a function of the stop mass. A scan of the mass spectrum in 1 GeV steps was performed using a sliding window of $\pm 2\sigma_{M_{\tilde{t}}}$ for $M_{\ell X} < 250$ GeV ($\ell = e$ or ν), where $\sigma_{M_{\tilde{t}}}$ is the stop mass resolution. For masses larger than 250 GeV, where the SM background is smaller and the expected signal width larger, the condition $M_{\ell X} > M_{\tilde{t}} - 2\sigma_{M_{\tilde{t}}}$ was applied.

At each stop mass, the 95% CL limit on λ'_{131} was evaluated using, for each channel, the data events, the SM predictions and the signal expectation for the corresponding mass window. The signal cross section was calculated in the NWA (Eq. 2) including initial state radiation (ISR) for the incoming proton [3] and the next-to-leading-order (NLO) QCD [4] corrections using the CTEQ6 set of parton densities, while the branching ratios for the different channels and MSSM scenarios were taken from the SUSYGEN simulation. The total likelihood was evaluated as the product of the Poissonian likelihoods of each channel. A Bayesian approach assuming a flat prior for the signal cross section was then used to produce the limits. The systematic uncertainties described in Section 6.1 have been included in the limit calculation assuming Gaussian distributions for their probability densities.

Figure 6 shows the 95% CL limit on λ'_{131} as a function of the stop mass for the range $-300\,\text{GeV} < \mu < 300\,\text{GeV}$, $100\,\text{GeV} < M_2 < 300\,\text{GeV}$ and $2 < \tan\beta < 50$. The limits for masses up to 250 GeV improve on the low-energy constraints from atomic parity violation (APV) [33] measurements (dashed line) and do not depend strongly on the different SUSY scenarios. The H1 collaboration obtained similar constraints [34] using similar SUSY scenarios.

6.3 Limits for mSUGRA model

For fixed values of λ'_{131}, constraints on the mSUGRA parameters can be set in the plane (m_0,$m_{1/2}$), when tanβ, A_0 and the sign of μ are fixed. The parameter A_0 enters only marginally at the electroweak scale and was set to zero. Limits at 95% CL were evaluated using a scan of the reconstructed mass spectrum and the same Bayesian approach as in the MSSM case.

Figure 7 shows the 95% CL exclusion limit area in the plane (m_0,$m_{1/2}$) for λ'_{131}=0.3, $\tan\beta = 6$ and $\mu < 0$ (hatched area). The dark region corresponds to values of parameters where no REWSB solution is possible, while the light region corresponds to neutralino masses (LSP) less than 30 GeV already excluded by LEP [6]. The dashed lines indicate the curve of constant stop mass close to the border of the excluded area. Limits can exclude stop masses up to 250 GeV for m_0 smaller than 230 GeV.

A scan towards large $\tan\beta$ has been performed assuming $M = m_0 = m_{1/2}$. Figure 8 shows the limits on M as a function of $\tan\beta$ for λ'_{131}=0.3 and $\mu < 0$. The limit on M is almost constant around 135 GeV up to $\tan\beta \sim 35$. For larger values, it drops due to the large mixing in the $\tilde{\tau}$ sector which results in a light $\tilde{\tau}_1$ state. Such a light $\tilde{\tau}_1$ enters in the stop decay chain, decreasing the signal efficiency. The H1 collaboration obtained comparable constraints [34] using the same mSUGRA scenarios.

6.4 Comparison to results from other colliders

Studies on stop in $\not{R}_p$ SUSY scenarios have been performed both at LEP [36–38] and the Tevatron [39], looking for the production of stop pairs. LEP mass limits for the stop, in the case of $\lambda' > 0$, were obtained by the OPAL [36] and ALEPH [37] collaborations and are in the range $85 - 98$ GeV. The CDF collaboration [39] set a stop mass limit at 122 GeV assuming $\lambda'_{33k} > 0$ and a branching ratio $B(\tilde{t} \to b\tau) = 1$.

A more interesting comparison between HERA and Tevatron sensitivities can be done looking at Tevatron results for leptoquark (LQ) production. The D0 Collaboration published limits on leptoquark masses as a function of the branching ratio $B(LQ \to eq)$ [40]. Since leptoquarks and squarks have analogue production mechanism, such limits can be converted into limits on the stop mass as a function of λ'_{131} and directly compared with the results of this analysis. In the case of the MSSM scenarios, D0 limits are competitive with those of HERA only for the largest values of M_2 and $|\mu|$, where the $\not{R}_p$ decay $\tilde{t} \to eq$ dominates due to the large chargino mass. For lower values of M_2 or $|\mu|$ the gauge stop decays are relevant and the ZEUS limits improve over those from D0 for masses larger than 150 GeV. Figure 9 shows the comparison between ZEUS and D0 limits for three different regions of the unconstrained MSSM parameter space. In the mSUGRA scenarios considered here, the gauge stop decays are always relevant and thus the ZEUS limits are more stringent than the D0 ones.

7 Conclusions

A search for stop production in e^+p collisions at HERA was performed using an integrated luminosity of 65 pb^{-1}. No evidence was found for resonances in the decay channels with jet(s) and one high-P_T positron or neutrino. The results have been interpreted in the framework of the R-parity-violating MSSM, setting limits on the Yukawa coupling λ'_{131} as a function of the stop mass. These limits exhibit a weak dependence on the MSSM parametes μ, M_2 and $\tan\beta$ and improve on limits from Tevatron in a large part of the considered parameter space, and on limits from low-energy APV measurements for stop masses lower than 250 GeV. Direct limits on the stop mass have also been derived within the mSUGRA model. In this model only five free parameters determine the full supersymmetric mass spectrum. In this case, for $\lambda'_{131} = 0.3$, stop with masses as high as 260 GeV are excluded for a large part of the parameter space.

References

[1] Y. A. Golfand and E. P. Likhttman, JETP Lett. **13**, 323 (1971);
D. V. Volkov and V. P. Akulov, JETP Lett. **16**, 438 (1972);
D. V. Volkov and V. P. Akulov, Phys. Lett. **B 46**, 109 (1973);
J. Wess and B. Zumino, Nucl. Phys. **B 70**, 39 (1974).

[2] J. Butterworth and H. Dreiner, *R-Parity Violation at HERA*, Nucl. Phys. **B 397**, 3 (1993).

[3] C.F. Weizsäcker, Z. Phys. **88**, 612 (1934);
E.J. Williams, Phys. Rev. **45**, 729 (1934).

[4] T. Plehn et al., Z. Phys. **C 74**, 611 (1997).

[5] H.K. Dreiner, *Perspectives on Supersymmetry*, Ed. by G.L. Kane, World Scientific, hep-ph/9707435.

[6] L3 Coll., M. Acciarri et al., Eur. Phys. J. **C 19**, 397 (2001).

[7] N. Polonsky, *Supersymmetry: Structure and Phenomena*, hep-ph/0108236.

[8] R. Barbieri, S. Ferrara and C. A. Savoy, Phys. Lett. **B 119**, 343 (1982);
L. J. Hall, J. Lykken and S. Weinberg, Phys. Rev. **D 27**, 2359 (1983);
P. Nath, R. Arnowitt and A. H. Chamseddine, Nucl. Phys. **B 227**, 121 (1983).

[9] ZEUS Coll., U. Holm et al., *The ZEUS Detector*. Status Report (unpublished), DESY (1993), available on `http://www-zeus.desy.de/bluebook/bluebook.html`.

[10] N. Harnew et al., Nucl. Inst. Meth. **A 277**, 176 (1989);
B. Foster et al., Nucl. Inst. Phys. Proc. Suppl. **B 32** 181 (1993);
B. Foster et al., Nucl. Inst. Meth. **A 338**, 254 (1994).

[11] M. Derrick et al., Nucl. Inst. Meth. **A 309**, 77 (1991);
A. Andresen et al., Nucl. Inst. Meth. **A 309**, 101 (1991);
A. Caldwell et al., Nucl. Inst. Meth. **A 321**, 356 (1992);
A. Bernstein et al., Nucl. Inst. Meth. **A 336**, 23 (1993).

[12] J. Andruszków et al., *First measurement of HERA luminosity by ZEUS lumi monitor.* Preprint DESY-92-066, DESY, 1992;
ZEUS Coll., M. Derrick et al., *Measurement of the total and partial photon proton cross section at 180 GeV center of mass energy.* Z. Phys. **C 63**, 391 (1994);
J. Andruszków et al., *Luminosity measurement in the ZEUS experiment.* Acta Phys. Pol. **B 32**, 2025 (2001).

[13] T. Sjostrand et al., Comp. Phys. Commun. **135**, 238 (2001).

[14] A. Kwiatkowski, H. Spiesberger and H. J. Mohring, *HERACLES 4.4*, Comp. Phys. Comm. **69**, 155 (1992).

[15] K. Charchula, G.A. Schuler and H. Spiesberger, Comput. Phys. Commun. **81**, 381 (1994).

[16] CTEQ Coll., H. L. Lai et al., Eur. Phys. J. **C 12**, 375 (2000).

[17] L. Lönnblad, Comput. Phys. Commun. **71**, 15 (1992).

[18] G. Ingelman, A. Edin and J. Rathsman, *LEPTO 6.1*, Comp. Phys. Comm. **101**, 108 (1997).

[19] T. Sjöstrand, Comput. Phys. Commun. **39**, 347 (1986);
T. Sjöstrand and M. Bengtsson, Comput. Phys. Commun. **43**, 367 (1987);
T. Sjöstrand, Comput. Phys. Commun. **82**, 74 (1994).

[20] G. Marchesini et al., Comp. Phys. Comm. **76**, 465 (1992).

[21] CTEQ Coll., H. L. Lai et al., Phys. Rev. **D 55**, 1280 (1997).

[22] M. Gluck et al., Phys. Rev. **D 46**, 1973 (1992).

[23] N. Ghodbane et al., *SUSYGEN 3.* hep-ph/9909499.

[24] J. Pumplin et al., JHEP **0207**, 012 (2002).

[25] ZEUS Coll., S. Chekanov et al., Phys. Rev. **D 68**, 052004 (2003).

[26] ZEUS Coll., S. Chekanov et al., Phys. Rev. **D 70**, 052001 (2004).

[27] ZEUS Coll., S. Chekanov et al., Eur. Phys. J. **C 32**, 16 (2003).

[28] ZEUS Coll., J. Breitweg et al., Z. Phys. **C 74**, 207 (1997).

[29] S. Bentvelsen, J. Engelen and P. Kooijman, *Proc. of the Workshop on Physics at HERA*, W. Buchmüller and G. Ingelman (eds.), Vol 1, p.23. Hamburg, Germany, DESY (1992).

[30] F. Jacques and A. Blondel, *Preceedings of the Study for an ep Facility for Europe.* U. Amaldi (ed.), p. 391. Hamburg, Germany (1979).

[31] G. Ingelman, A. Edin and J. Rathsman, Comput. Phys. Commun. **101**, 108 (1997).

[32] CTEQ Coll., H.L. Lai et al., Phys. Rev. **D 55**, 1280 (1997).

[33] P. Langacker, *Parity violation in muonic atoms and cesium.* Phys. Lett. **B 256**, 277 (1991).

[34] H1 Coll., A. Aktas et al., Eur. Phys. J. **C 36**, 425 (2004).

[35] A. Djouadi, J. Kneur and G. Moultaka, *SuSpect: a Fortran Code for the Supersymmetric and Higgs Particle Spectrum in the MSSM*, hep-ph/0211331.

[36] Opal Coll., G. Abbiendi et al., Eur. Phys. J. **C 33** 149 (2004).

[37] Aleph Coll., A. Heister et al., Eur. Phys. J. **C 31** 1 (2003).

[38] L3 Coll., P. Achard et al., Phys. Lett. **B 524**, 65 (2002).

[39] CDF Coll., D. Acosta et al., Phys. Rev. Lett. **92**, 051803 (2004).

[40] D0 Collab., V.M. Abazov et al., Phys. Rev. D Rapid Comm. **71**, 071104(R) (2005).

Channel	y_{cut}	$P_{T,\mathrm{antipar}}/P_{T,\mathrm{par}}$	Data	SM	Eff. MSSM
e-J	$0.4 - 0.7$	< 0.05	85	$74.5^{+2.6}_{-7.2}$	0.3
e-MJ	$0.4 - 0.7$	> 0.05	63	$58.8^{+2.1}_{-9.0}$	0.15-0.2
ν-MJ	0.6	> 0.1	19	$20.9^{+1.7}_{-2.9}$	0.15-0.35

Table 1: *Summary of final selection cuts, number of observed and expected events and signal efficiencies for MSSM ($M_{\tilde{t}} = 220$ GeV) for the different channels.*

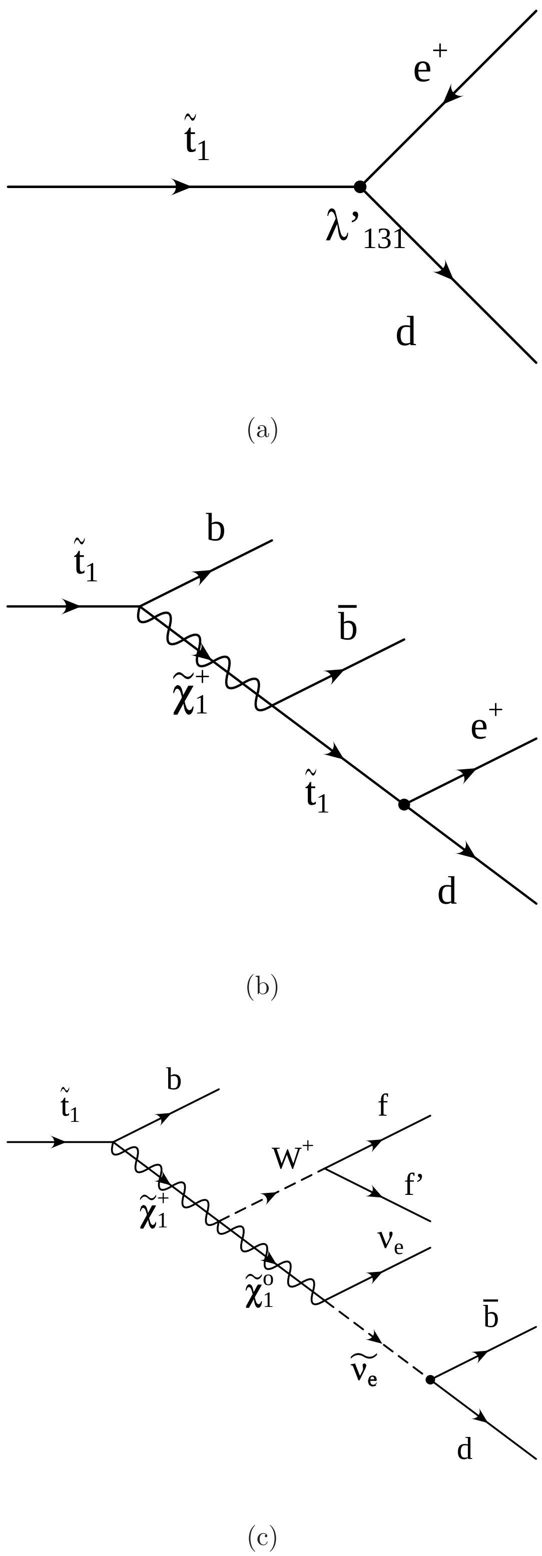

Figure 1: *Considered decay modes of the stop squark: (a) the e-J channel, (b) the e-MJ channel and (c) the ν-MJ channel.*

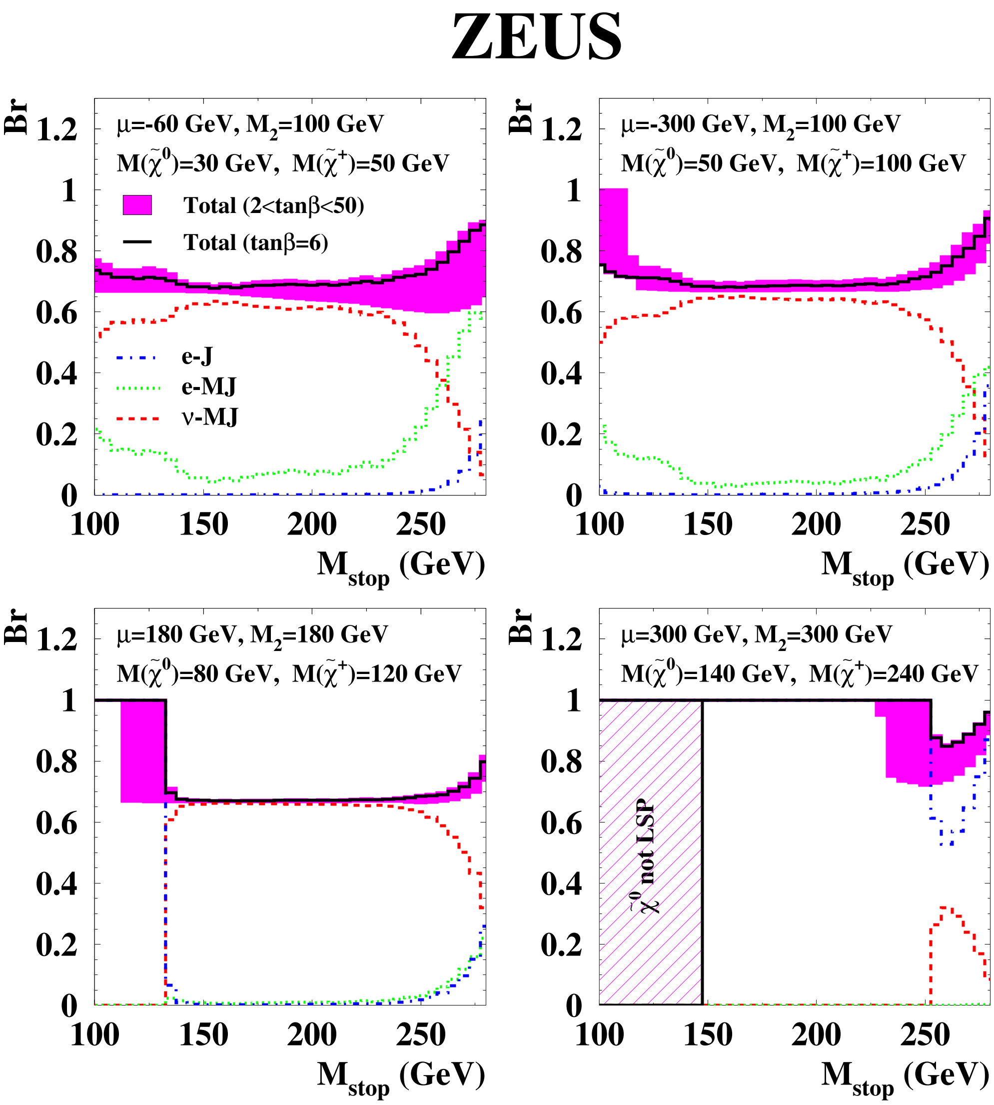

Figure 2: *Branching ratios as a function of the stop mass for different μ and M_2 values, and for λ'_{131} equal to the ZEUS limit for the considered scenarios. The three channels considered in the analysis and their sum are shown for* $\tan\beta = 6$. *The dark band is the range of the total branching ratio for* $2 < \tan\beta < 50$.

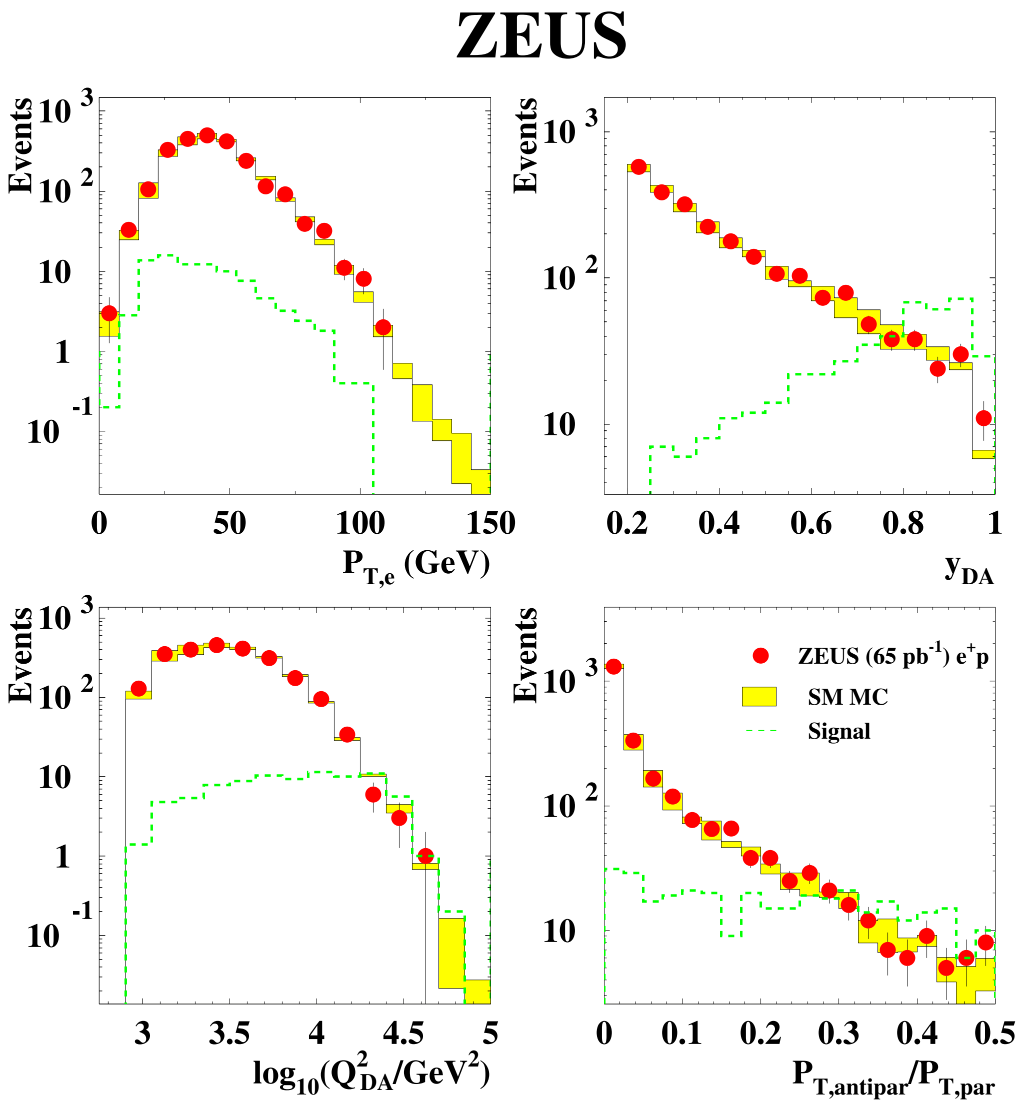

Figure 3: *Comparison between data (dots) and SM MC (histograms) for $P_{T,e}$, y_{DA}, $\log_{10}(Q^2_{DA})$ and $P_{T,antipar}/P_{T,par}$. The band represents the uncertainty on the SM expectation. The MSSM signal for the e-MJ channel (dashed line) with $M_{\tilde{t}} = 220\ GeV$, $M_2 = 100\ GeV$ and $\mu = -300\ GeV$ is also shown with arbitrary normalization.*

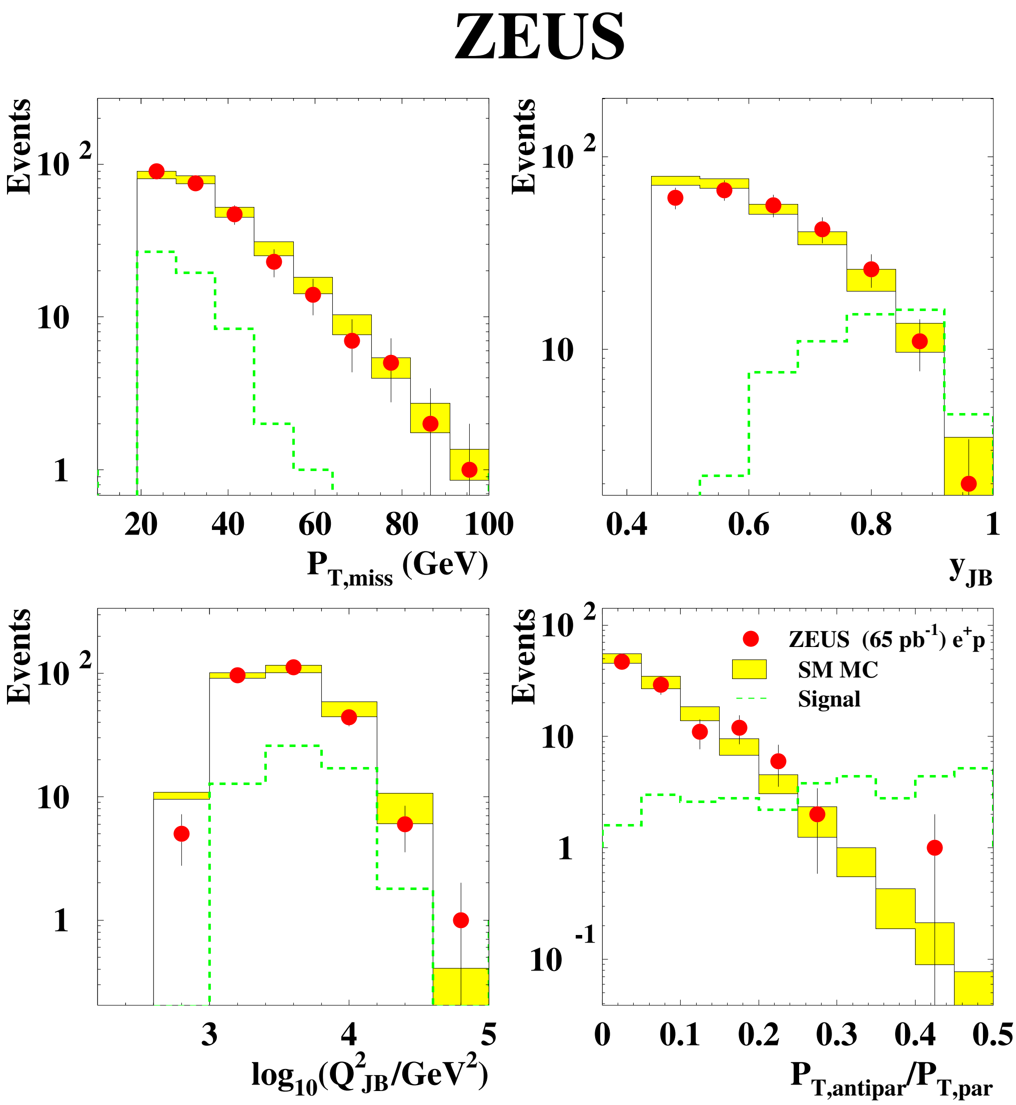

Figure 4: *Comparison between data (dots) and SM MC (histograms) for* P_T*,* y_{JB}*,* $\log_{10}(Q^2_{JB})$ *and* $P_{t,antip}/P_{t,par}$*, where the band represents the uncertainty on the SM expectation. The MSSM signal channel (dashed line) with* $M_{\tilde{t}} = 220$ *GeV,* $M_2 = 100$ *GeV and* $\mu = -300$ *GeV is also shown with arbitrary normalization.*

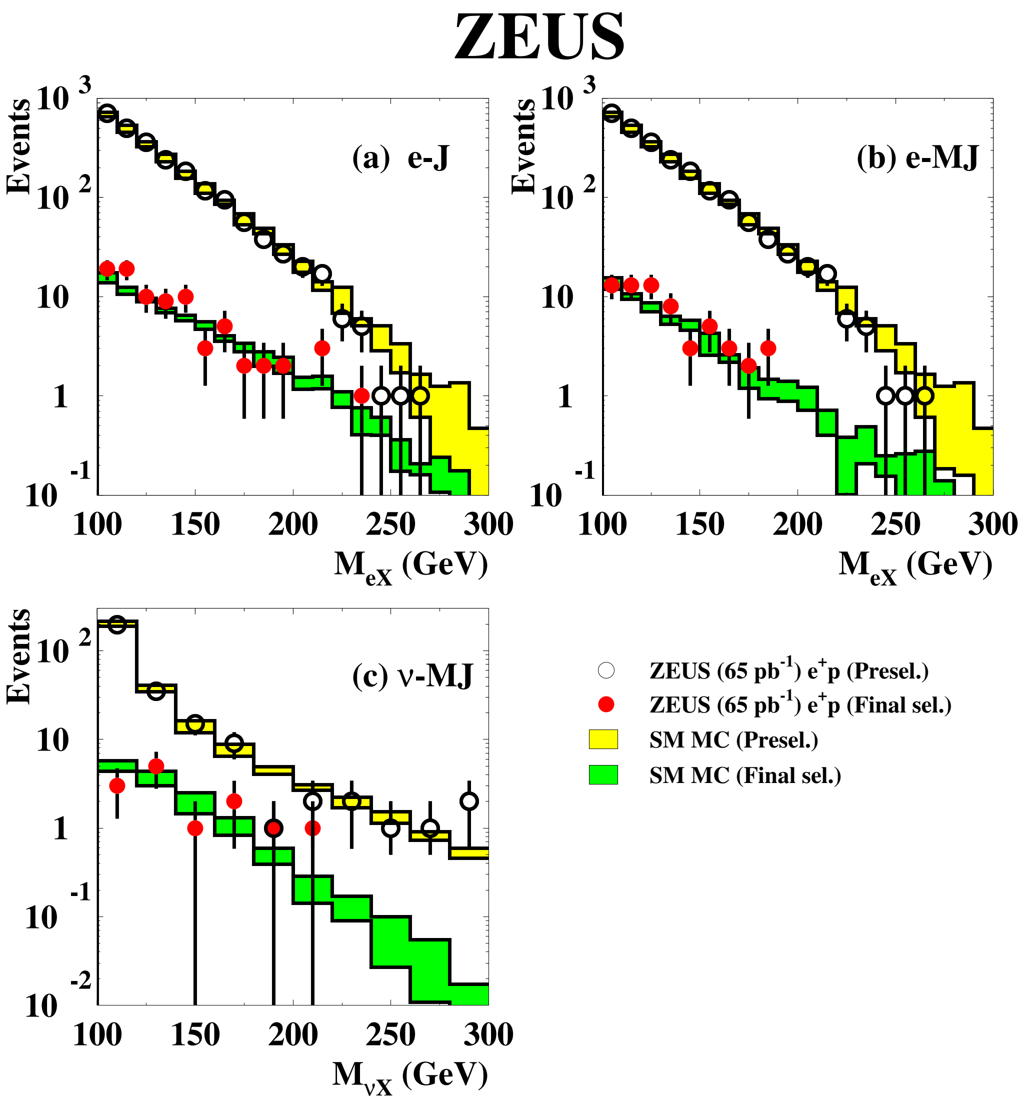

Figure 5: *Invariant mass for (a) e-J, (b) e-MJ and (c) ν-MJ distributions. The data (dots) and SM MC (histograms) after preselection (empty circles and light histograms) and final selection (filled circles and dark histograms) are shown. The bands represent the uncertainty on the SM expectation.*

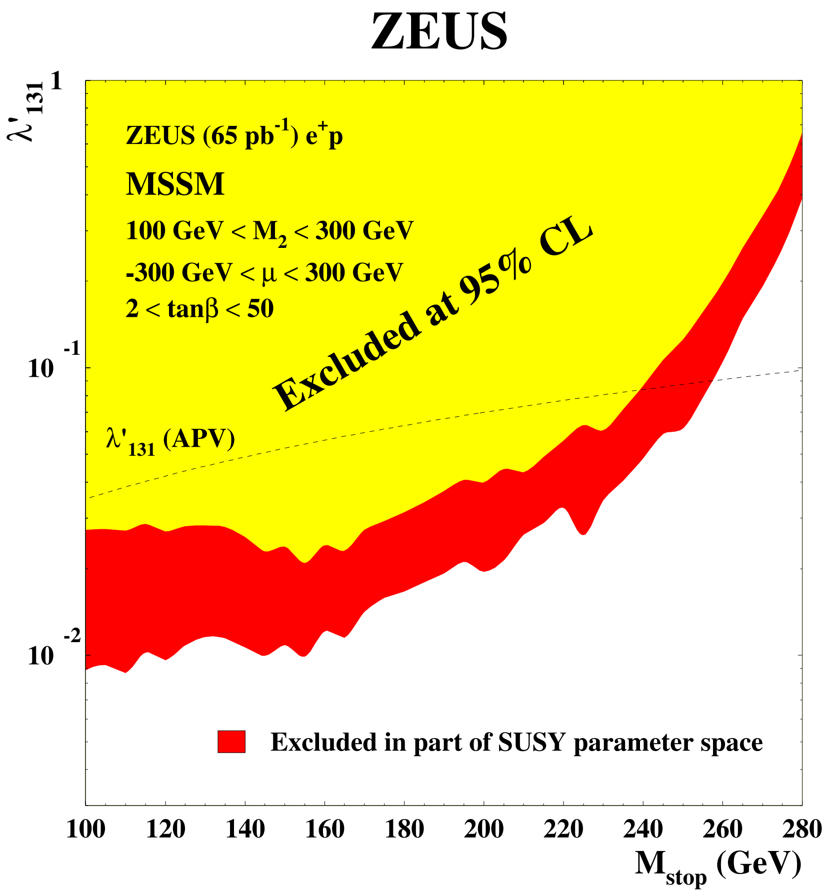

Figure 6: *Exclusion limits on λ'_{131} as a function of the stop mass. The light (dark) region is excluded in all (part of the) considered SUSY parameter space. The limit from low-energy APV measurements is also shown.*

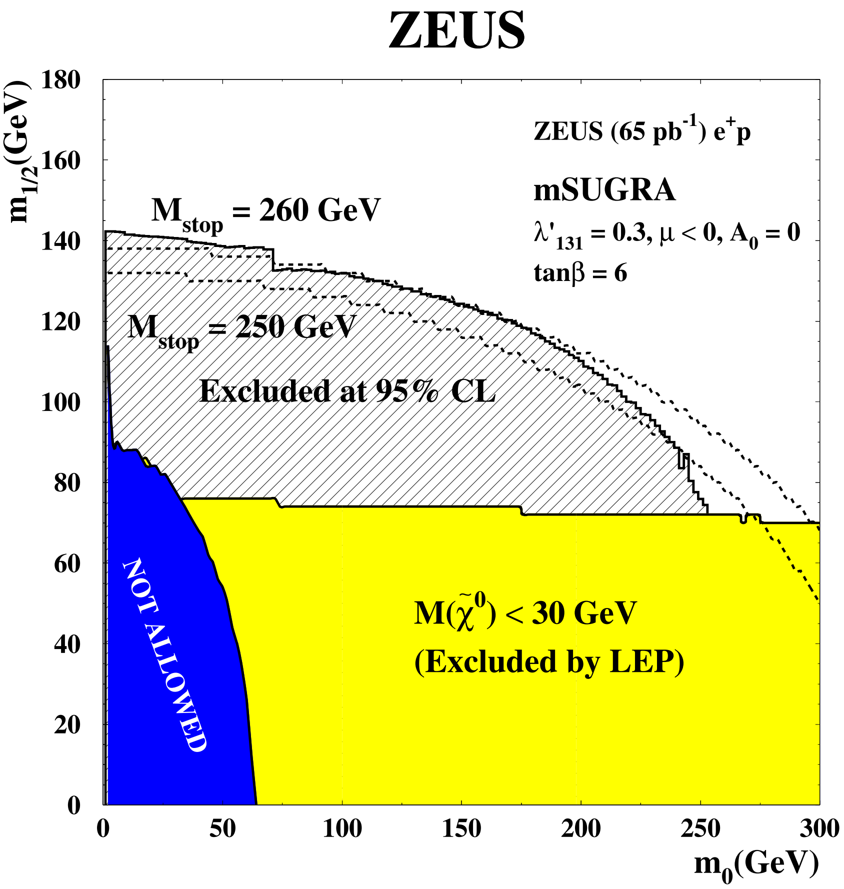

Figure 7: *Exclusion limits (95% CL) for mSUGRA with tanβ=6, λ'_{131}=0.3 and $\mu < 0$ (dashed area). The dark-shaded region corresponds to values of parameters where no radiative electro-weak symmetry breaking solution is possible. The light-shaded region corresponds to neutralino masses (LSP) less than 30 GeV, already excluded by LEP results. The dashed lines indicate the curve of constant stop mass close to the border of the excluded region.*

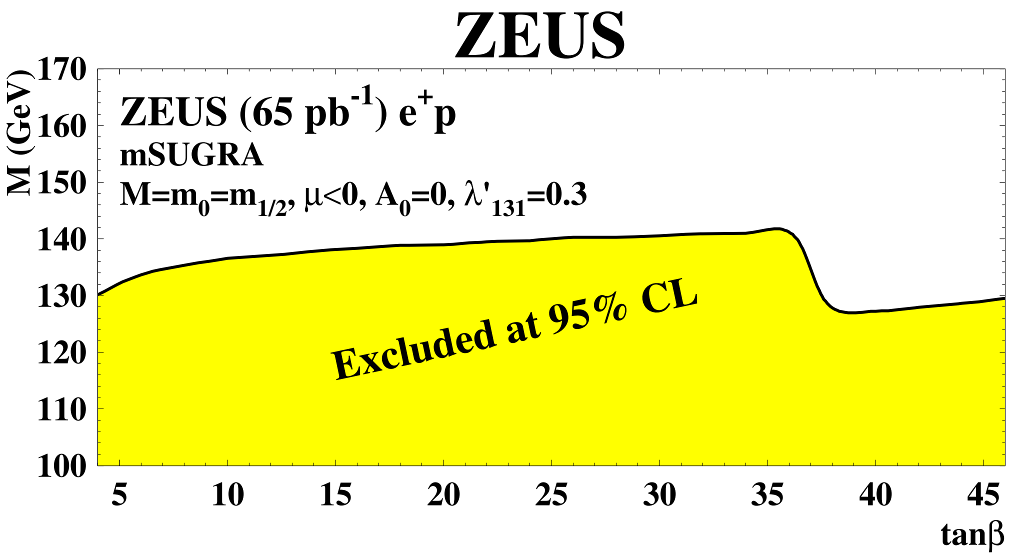

Figure 8: *Exclusion limit for mSUGRA on the mass parameter M* $(M = m_0 = m_{1/2})$ *as a function of* $\tan\beta$ *for* λ'_{131}*=0.3 and* $\mu < 0$.

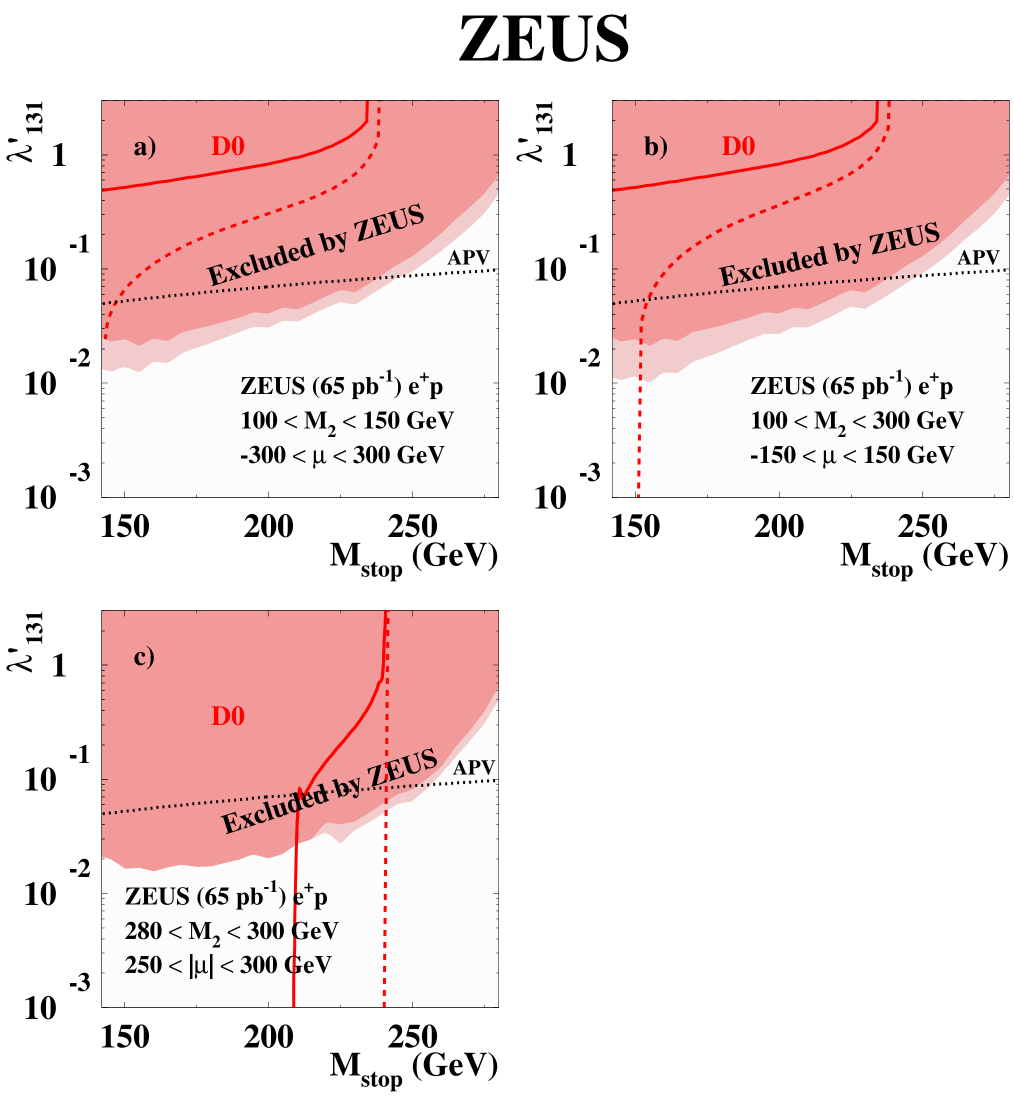

Figure 9: *Comparison between ZEUS, D0 and APV limits in the MSSM scenario for low M_2 (a), low $|\mu|$ (b) and high M_2 and $|\mu|$ (c). The regions excluded by ZEUS and D0 are shown by the dark-shaded area and by the area above the full line, respectively. The regions excluded in part of the parameter space are the light-shaded area (ZEUS) and the area between the full and the dashed line (D0). The region of exclusion for APV is above the dotted line.*